BSc Advanced Technology
Bachelor Assignment

Estimation of vertical ground reaction force using a single IMU located on the sternum

Jasper van den Berg

Supervisor: dr.ir. B.L. Scheltinga

July, 2025

Department of Biomedical Signals and Systems
Faculty of Electrical Engineering,
Mathematics and Computer Science
University of Twente

UNIVERSITY OF TWENTE.

Contents

1 Abstract

Ground reaction force (GRF) measurements provide insight into biomechanical load. This helps manage load and reduce injury risk. Currently measurement of the ground reaction force is restricted to laboratory settings. To estimate ground reaction force in other environments IMU's can be used to track the runners movement from which the ground reaction force can be estimated. The goal of this study is to estimate ground reaction force using a single IMU located on the sternum, with the end goal of improved injury prevention. This study explores the application of a mass, spring, damper model where the ground reaction force is estimated using a dual-Kalman filter. This method has the benefits of dynamic estimation of the model parameters as well as the unknown input. For this study 13 participants ran at a speed of $10km/h$ at their preferred stride frequency. GRF estimates were validated against an instrumented treadmill. Accuracy was measured using RMSE, peak errors, and Pearson's r with results: an RMSE of $0.214BW$, absolute mean peak error of $0.1000BW$, relative mean peak error of 4.500% and a Pearson's coefficient of 0.96. Though outperformed by current methods, it shows promise for future single-sensor GRF estimation.

2 Introduction

Over the last decades the knowledge about the health risks of an inactive lifestyle increased significantly. Physical activity is widely regarded to have a positive influence on personal health. Physical activity reduces the chance of getting several chronic conditions including stroke, type 2 diabetes and multiple types of cancer [1]. Furthermore, people who regularly engage in physical activity are less likely to struggle with different types of anxiety as well as depression [2]. The growth in knowledge of the effects of physical activity and the dangers of inactivity has lead to a growth in concerns about the inactive lifestyle large parts of the population partake in. In spite of this a large part of the population still engages in insufficient amounts of physical activity. In the Netherlands only 45% of the population of 4 years and older reached the recommended amount of physical activity in 2023 [3].

Running is one of the most popular sports in the world. Taking up a spot in the top 5 most popular sports in all regions of the world [4]. The low barrier of entry makes running a great sport to adopt when working towards a healthy lifestyle. Furthermore, running is also a large part of many other sports such as football, field hockey, etc. Apart from the general benefits of physical activity, the effects of running on personal health have also been studied widely. Runners have reduced all-risk as well as cardiovascular mortality [5]. Where the amount of running is related to the reduction in mortality risk. However, low amounts of running are enough to clearly see a reduction in mortality risk. In addition to this, the mental benefits of running are in line with the benefits of general physical activity, as they decrease the chance of anxiety and depression and can positively influence mood [6] [7].

Running has a lot of positive benefits however, many runners still quit running at some point. When inquired through a survey the main reason ex-runners gave for quitting was labeled "physical constraints and injuries" [8]. Over the course of a year between 27% and 70% of runners experience some kind of injury [9]. The injuries sustained during running can be divided into two categories. These are acute injuries such as sprains and fractures and overuse injuries which are caused by fatigue build up over time. Most injuries obtained during running fall into the second category, where most injuries occur in the knee, ankle, foot, and lower leg due to repetitive fatigue build-up. Fatigue builds up when stress is applied to a material. Biological tissue responds to stress by repairing and strengthening the tissue [10]. However, too much stress causes excessive build-up of fatigue. Stress needs to be managed to ensure fatigue does not build up to a level that will result in an injury. Injuries can lead to an inability to participate in physical activity and, as stated, is one of the main reasons people stop running. Since this would eliminate all of the benefits of physical exercise mentioned above, it is crucial to find ways to improve methods of injury prevention.

The most direct and generally applicable method of preventing overuse injuries is managing the accumulation of fatigue. The management of fatigue is done through proper dosage of running and other physical activity as the amount of fatigue is mainly related to a combination of intensity and frequency of exercise. To ensure a proper dosage of training it is important to know the amount of fatigue gathered in your body during training sessions. Since it is difficult to measure the amount of fatigue built up directly, it is useful to estimate the load placed on the body since this is related to the amount of fatigue added to your body. One of the measures that can be used to quantify biomechanical load is the ground reaction force (GRF) [11]. This is the force that the ground exerts on the body when they come in contact. Next to the direct insight into biomechanical load from GRF, it can also be used to estimate the load on specific parts of the body through biomechanical models, in this way the amount of load on a specific (possibly injury prone) part of the body can be estimated. Measurement of the GRF during running can help determine optimal amounts of rest and training intensity to reduce the chance of overuse injuries.

Most GRF measurements are currently done in a laboratory with the use of an instrumented treadmill or force plates [12]. With these methods it is possible to directly measure the GRF. This does however come with the drawback of restricting the measurements to a laboratory. The results gathered in the lab are very accurate but can not be directly assumed to be the same as the GRF's a runner experiences during a run outside where variables such as running surface and different running form influence the GRF significantly, the influence of this is even greater when looking at running related sports where direction changes are common. Furthermore, it would be useful for managing fatigue to be able to measure the GRF during any training session which will most often occur outside of the lab. This gives rise to the desire to estimate GRF using a wearable device.

The ground reaction force can be split in three directions (mediolateral, posterior-anterior, vertical). Of these directions the vertical direction contains the largest part of the force. A vertical ground reaction force (vGRF) waveform typically consists of a passive and an active peak [13]. The passive peak is caused by the initial impact absorbed in the body, the active peak is caused by the force exerted by the runner to propel themselves forward. The passive peak is mostly absorbed in the lower body while the active peak is more prevalent in the entire body [14]. Running form has a large influence on the GRF waveform. Heel-strike runners land with their heel first where they absorb the first impact after which they roll onto their forefoot and exert force to propel themselves forward, forefoot-strike runners land on their forefoot where they both absorb impact and generate force. Because of this the impact peak is not present for forefoot strike runners while it is prevalent in heel-strike runners [15]. Mid-foot strike runners GRF pattern usually is a combination of the aforementioned running styles.

There are multiple types of sensors and methods that are currently used to estimate GRF. Firstly the measurement of force through force sensors in the insoles of a runner. In this method sensors are placed throughout the insole to directly measure pressure distribution and force wave patterns during running [16]. While this method currently reaches the highest accuracy in the area of wearable sensors [17] this method does come with some downsides. Adding sensors in the insole of a shoe can change the feel and stiffness of the shoe causing a change in the running pattern. Furthermore, these sensors are repeatedly loaded with significant amounts of force which leads to a low lifespan.

Secondly, optical motion capture technology is used to measure the movement pattern of a runner. From this the GRF can be estimated in different methods, one method is using a neural network to estimate the GRF based on the measured movement [18]. This can be an effective method and is applicable to many team sports where cameras can be set up around the playing field. For running it is more difficult to implement since there is no defined environment.

The third method commonly used for GRF estimation makes use of IMU's (inertial measurement unit) to track the movement of different body segments, these sensors combine accelerometer, gyroscope, and sometimes magnetometer data to give measurements on acceleration, velocity, and orientation. To properly track a runners movement, sensors are attached to multiple relevant body segments, these locations usually consist of some combination of both feet, both tibias, both thighs, pelvis, and sternum [19] [20]. To estimate the GRF from inertial sensor data there are multiple methods available. The most prevalent ones are estimation through the use of an artificial neural network [21] and estimation using a biomechanical model [19] and filtering. A simple example of the second variation is the Newtonian method, it implements newtons second law directly on the measured acceleration, as successfully demonstrated by Scheltinga et al. [19]. Another variation of this second method is implemented by Leblanc et al. [12], where a dual-Kalman filter is used to estimate the states and parameters of a biomechanical model from which the GRF can be calculated. The Kalman filter is a state estimation technique which combines measurements related to the states of a model with the behavior predicted by the the models state equations [22]. The dual-Kalman filter structure consists of an unscented Kalman filter and a regular Kalman filter. Here the first is used for estimation of the states and the model parameters, as the unscented Kalman filter is able to deal with the non-linearity of the model due to its varying parameters. The second is used to deal with the unknown system input.

On the road to estimating GRF using wearable devices for general consumption it is important to review the trade-off that occurs when adding and removing sensors. A larger number of sensors gives more information on the motion of different body parts which will lead to a more accurate estimation of the GRF [17]. The addition of more sensors does lead to a decrease in comfort and ease of use which is very relevant with the context of general use in mind. The goal of this project is set up around GRF estimation based on a single inertial sensor placed on the sternum of the runner. This sensor setup is chosen with the goal of high ease of use, as runners already often wear a heart-rate monitor near this location. This could later be easily translated to other single sensor torso based setups due to the rigidity of the torso. Because a single sensor located on the torso carries limited information about the forces absorbed in the lower body a biomechanical model based method is chosen for this study as this can help predict unmeasured behavior of the model. The dual-Kalman filter method introduced above will be used to estimate the GRF. Compared to the Newtonian method this method should allow implementation of a more accurate model where the forces absorbed in the lower body are accounted for. Furthermore, compared to a single Kalman state estimator the dual-Kalman filter allows for estimation of the unknown input. This should better deal with unpredictable external forces applied to the runner and thus improve performance. The dual-Kalman filter model has previously been applied successfully by Leblanc et al. [12] using a single sensor placed on the sacrum. The goal of this study is to evaluate whether this method is applicable to a single sternum sensor setup with the end goal of improved injury prevention through accurate GRF estimation. To validate the model the estimated GRF is compared to the measured GRF obtained using an instrumented treadmill. To quantify the performance of the dual-Kalman filter method several error metrics will be compared to a straight forward Newtonian method using the same data as well as other presented literature. In this report the applied method, its results and their interpretation will be presented.

3 Method

3.1 Experimental design and measurement setup

The data used in this study was gathered as part of a larger study aimed at estimating biomechanical parameters from IMU data. In this study 13 runners participated in the measurements, this includes 9 male and 4 female runners with the following properties: age $31.2 \pm 8.9y$, height $1.83 \pm 0.10m$, weight $76.03 \pm 15.79kg$

During the measurement, first parameters such as age and height were gathered, after which the weight was measured. After this the running trials started, each trial started and ended with the participant jumping 3 times. Participants ran at three different speeds (10, 12 and 14 km/h) and three different stride frequencies (90, 100 and 110% of preferred stride frequency). Each trial consisted of $40s$ ramp up, $40s$ running at speed and $10s$ of slowing down. In between the trials the participants rested for 3 minutes to prevent them from fatiguing excessively. For the scope of this study only the measurement at $10km/h$ at preferred stride frequency is used.

The trials were completed using IMU sensors (MVN Link, XSENS, Enschede, The Netherlands) to capture the movement of different segments on the body. For this study only the IMU placed on the sternum is used. These sensors have a sampling frequency of $240Hz$. The sensor are attached using double sided tape, an additional layer of tape was used on top of the sensors to reduce movement artifacts in the sensor data.

A 3D instrumented dual-belt treadmill (custom Y-mill, motekforce link, Culemborg, The Netherlands) was used to collect the reference GRF. This system has a sampling frequency of $2048Hz$.

3.2 Data processing

The data from the instrumented treadmill is filtered using a low pass 3rd order Butterworth filter with a cut-off frequency of $30Hz$. This signal is then downsampled to the frequency of the IMU. The measurements are then aligned using the jumps at the start and end of the measurements. From the middle of the trials 40 strides were extracted to be used in the GRF estimation and its validation. Both the data from the instrumented treadmill and the estimated GRF were normalized to body weight. To make a distinction between the stance and flight phase, the data is labeled as flight phase if the measured GRF $< 25N$ for longer than $0.05s$ and as stance phase if the measured GRF $> 25N$ for longer than $0.05s$. The MVN Link system outputs different preprocessed accelerations, for this study the sensor free acceleration is used which is acceleration in the global frame without gravity included.

3.3 Model

The biomechanical model used to predict the ground reaction force is a mass spring damper (MSD) model, shown in Figure 1. This model is used in many instances to estimate locomotive mechanics, mainly used for predicting and characterizing the mechanics of bouncing gaits such as running [23][24]. The vertical component of the GRF contains a significantly higher portion of the total GRF compared to the other two components. To restrain complexity while keeping an accurate measure of the GRF this study is constrained to estimating only the vertical component and can thus be modeled using a single degree of freedom mass, spring, damper system.

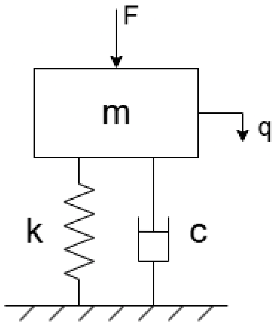

FIGURE 1: Mass spring damper model, where k is the stiffness, c the damping and m the mass

This model is characterized by the following differential equation:

$$m\frac{d^2q}{dt^2}(t) + c\frac{dq}{dt}(t) + kq(t) = u(t) \tag{1}$$

Here m, c and k are the mass, damping and stiffness of the model respectively, q represents the displacement of the mass at time t and u the unknown input at time t.

The output (estimated GRF (eGRF)) is a sum of the forces acting on the ground, in this case these are the spring and damping forces:

$$eGRF = -kq - c\frac{dq}{dt} \tag{2}$$

3.4 State and input estimation

The states of the a mass spring system are typically as follows, $\mathbf{x} = [q\,\dot{q}]$. These states are not directly measured with the sternum IMU, while they are needed to calculate the estimated GRF and thus need to be estimated using the model introduced above.

The acceleration measured by the IMU closely matches the acceleration of the mass in the model shown above. While this allows for direct integration of the acceleration to estimate the states, this does not handle noise well and is unable to deal with the uncertainty of the structural mechanics caused by the unknown stiffness parameter. The use of a Kalman filter introduces optimized model-data fusion, which combines an estimate of the state based on the model and previous values of the states with the measurements to more accurately estimate the states of the system. Furthermore, the dual KF-UKF observer structure proposed by Dertimantis et al. [25] is able to deal with the uncertainty in the structural mechanics as well as the unknown input. The proposed dual KF-UKF filter structure is shown in Figure 2.

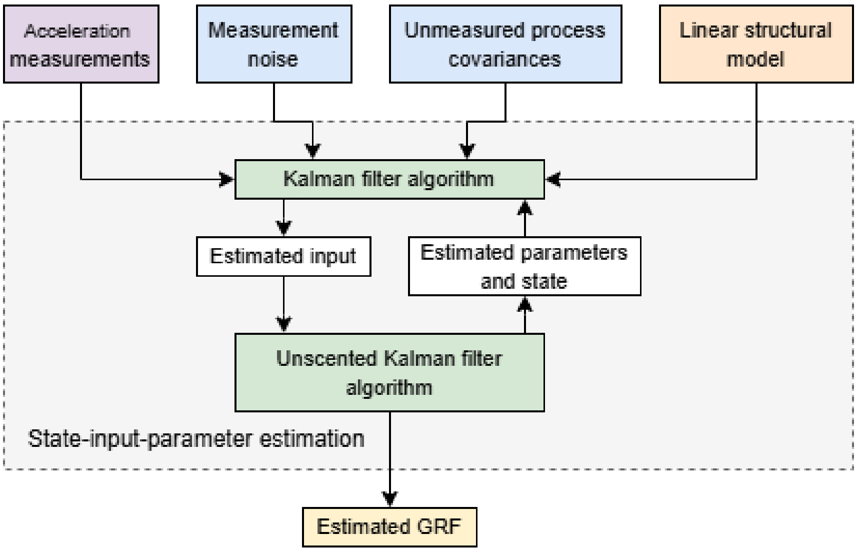

FIGURE 2: Dual KF-UKF filter structure used for vGRF estimation, previously demonstrated by Leblanc et al. [12]

The Kalman filter used for estimation the input of the structural model is executed through the following standard equations [22]:

Prediction step:

$$\hat{\mathbf{x}}_{k+1}^{-} = \mathbf{A}\hat{\mathbf{x}}_k \tag{3}$$

$$\mathbf{P}_{k+1}^{-} = \mathbf{A}\mathbf{P}_k\mathbf{A}^{\mathrm{T}} + \mathbf{Q} \tag{4}$$

Correction Step:

$$\mathbf{K}_k = \mathbf{P}_k^{-}\mathbf{H}^{\mathrm{T}}\left(\mathbf{H}\mathbf{P}_k^{-}\mathbf{H}^{\mathrm{T}} + \mathbf{R}\right)^{-1} \tag{5}$$

$$\hat{\mathbf{x}}_k = \hat{\mathbf{u}}_k^{-} + \mathbf{K}_k\left(\mathbf{z}_k - \mathbf{z}_{pred}\right) \tag{6}$$

$$\mathbf{P}_k = \left(\mathbf{I} - \mathbf{K}_k\mathbf{H}\right)\mathbf{P}_k^{-} \tag{7}$$

Where $\hat{\mathbf{x}}_k \in \mathbb{R}^{n\times 1}$ is the state, $\mathbf{P}_k \in \mathbb{R}^{n\times n}$ is the covariance matrix, $\mathbf{K}_k \in \mathbb{R}^{n\times m}$ is the Kalman gain and $\mathbf{A} \in \mathbb{R}^{n\times n}$, $\mathbf{H} \in \mathbb{R}^{m\times n}$, $\mathbf{Q} \in \mathbb{R}^{n\times n}$, $\mathbf{R} \in \mathbb{R}^{m\times m}$ are the state transition matrix, measurement matrix, process noise covariance and measurement noise covariance respectively. $\mathbf{z}_k \in \mathbb{R}^{m\times 1}$ and $\mathbf{z}_{\mathrm{pred}} \in \mathbb{R}^{m\times 1}$ are the measurements and predicted values of the measurements respectively. Here n and m are the amount of states and measurements, for this first filter $n = m = 1$.

The goal of this first filter is to estimate the input of the mass spring damper model and is thus processed as the state in this first filter, $\hat{\mathbf{x}}_k = [u_k]$. The state transition matrix describes the modeled evolution of the state, since the behavior of the input is unknown it is modeled using a 1st order linear autoregressive model, $\mathbf{A} = T$. The input is thus modeled by Equation 8:

$$\mathbf{u}_{k+1} = T\mathbf{u}_k \tag{8}$$

The only notable difference between the standard Kalman filter and this implementation is the calculation of $\mathbf{z}_{\mathrm{pred}}$. In a standalone Kalman filter this is calculated using the dot product of the measurement matrix and the state matrix. In the dual Kalman structure it is calculated similarly but using the states and the measurement models of both filters. This is where the feedback of parameters and state shown in Figure 2 is implemented.

The UKF is the second part of the total dual filter structure. Here the states and stiffness get estimated which are then used to produce an estimate of the GRF. The UKF consists of a similar recursive method to the KF containing a prediction and correction step. These steps are however applied on a select number of points instead of the whole distribution as is done in the KF. This change allows the handling of the time varying stiffness parameter. The filter starts of every loop selecting $2n+1$ sigma points as follows [26]:

$$\mathbf{X}^{[i]} = \begin{cases} \hat{\mathbf{x}} & i = 0 \\ \hat{\mathbf{x}} + \left[\sqrt{(n+\lambda)\mathbf{P}}\right]_i & i = 1, \ldots, n \\ \hat{\mathbf{x}} - \left[\sqrt{(n+\lambda)\mathbf{P}}\right]_{i-n} & i = n+1, \ldots, 2n \end{cases} \tag{9}$$

The Sigma points are then passed through the state transition model. To reproduce the state and covariance from the processed sigma points, they are assigned weights as follows [26]:

$$\mathbf{W}_m^{[i]} = \begin{cases} \frac{\lambda}{n+\lambda} & i = 0 \\ \frac{1}{2(n+\lambda)} & i = 1, \ldots, 2n \end{cases}, \quad \mathbf{W}_c^{[i]} = \begin{cases} \frac{\lambda}{n+\lambda} + (1 - \alpha^2 + \beta) & i = 0 \\ \frac{1}{2(n+\lambda)} & i = 1, \ldots, 2n \end{cases} \tag{10}$$

Here $\mathbf{W}_m^{[i]}$ are the weights for the state mean and $\mathbf{W}_c^{[i]}$ are the weights for the state covariance. Furthermore, α, β and κ are UKF parameters and $\lambda = \alpha^2(n+\kappa) - n$. The mean and covariance of the predicted states is determined according to Equation 11 [26].

$$\hat{\mathbf{x}}^- = \sum_{i=0}^{2n} \mathbf{W}_m^{[i]} \mathbf{X}^{[i]}, \quad \mathbf{P}_{xx} = \sum_{i=0}^{2n} \mathbf{W}_c^{[i]} \left(\mathbf{X}^{[i]} - \hat{\mathbf{x}}\right) \left(\mathbf{X}^{[i]} - \hat{\mathbf{x}}\right)^{\mathrm{T}} \tag{11}$$

$$\hat{\mathbf{z}} = \sum_{i=0}^{2n} \mathbf{W}_m^{[i]} \mathbf{Z}^{[i]}, \quad \mathbf{P}_{zz} = \sum_{i=0}^{2n} \mathbf{W}_c^{[i]} \left(\mathbf{Z}^{[i]} - \hat{\mathbf{z}}\right) \left(\mathbf{Z}^{[i]} - \hat{\mathbf{z}}\right)^{\mathrm{T}} \tag{12}$$

In the correction step the sigma points processed in the prediction step are fed through the measurement model. Again the weights are used to get the mean and covariance of the estimated measurement values according to Equation 12. After which the Kalman gain is determined and used to correct the state and its covariance matrix [26]:

$$\mathbf{P}_{xz} = \sum_{i=0}^{2n} \mathbf{W}_c^{[i]} \left(\mathbf{X}^{[i]} - \hat{\mathbf{x}}\right) \left(\mathbf{Z}^{[i]} - \hat{\mathbf{z}}\right)^{\mathrm{T}} \tag{13}$$

$$\mathbf{K} = \mathbf{P}_{xz} \mathbf{P}_{zz}^{-1} \tag{14}$$

$$\hat{\mathbf{x}} = \hat{\mathbf{x}}^- + \mathbf{K}\left(\mathbf{z} - \hat{\mathbf{z}}\right) \tag{15}$$

$$\mathbf{P} = \mathbf{P}^- - \mathbf{K}\mathbf{P}_{zz}\mathbf{K}^{\mathrm{T}} \tag{16}$$

This second filter is used to predict the states and the stiffness of the MSD system. The state space representation shown in Equation 17 is derived from Equation 1. The evolution of the stiffness is modeled as a random walk, shown in Equation 19.

$$\hat{\mathbf{x}}_{k+1}^{-} = \mathbf{A}\hat{\mathbf{x}}_k + \mathbf{B}\hat{\mathbf{u}}_k, \qquad \hat{\mathbf{z}}_{k+1} = \mathbf{C}\hat{\mathbf{x}}_k + \mathbf{D}\hat{\mathbf{u}}_k \tag{17}$$

$$\mathbf{A} = \begin{bmatrix} 0 & 1 \\ -\frac{k}{m} & -\frac{c}{m} \end{bmatrix}, \qquad \mathbf{B} = \begin{bmatrix} 0 \\ \frac{1}{m} \end{bmatrix}, \qquad \mathbf{C} = \begin{bmatrix} -\frac{k}{m} & -\frac{c}{m} \end{bmatrix}, \qquad \mathbf{D} = \begin{bmatrix} \frac{1}{m} \end{bmatrix} \tag{18}$$

$$k_{k+1}^{-} = k_k \tag{19}$$

The stiffness is included as an extra state in the augmented state vector resulting in the augmented state vector, augmented state transition model and the augmented measurement model shown in Equation 20, 21 and 22 respectively. These are the models used in the UKF.

$$\hat{\mathbf{x}}^{aug} = [q\, \dot{q}\, k] \tag{20}$$

$$\hat{\mathbf{x}}_{k+1}^{aug-} = \begin{bmatrix} \mathbf{A} & 0 \\ 0 & \mathbf{I} \end{bmatrix} \hat{\mathbf{x}}_k^{aug} + \begin{bmatrix} \mathbf{B} \\ 0 \end{bmatrix} \hat{\mathbf{u}}_k \tag{21}$$

$$\hat{\mathbf{z}}_{k+1} = \begin{bmatrix} \mathbf{C} & 0 \end{bmatrix} \hat{\mathbf{x}}_k^{aug} + \begin{bmatrix} \mathbf{B} \end{bmatrix} \hat{\mathbf{u}}_k \tag{22}$$

Combining the KF and UKF in an iterative process will apply the total dual filter architecture to the measured acceleration to estimate the states of the applied model. In this iterative process the vGRF is calculated at every state update using Equation 2. When combined, this results in the total eGRF waveform.

3.5 Parameter determination and optimization

To use the state estimation method described previously a number of parameters and initial values need to be determined. These are divided in the four categories. The following sections describe how these values are derived. The values used in the estimation of the vGRF can be found in Table 1.

3.5.1 Model parameters

Firstly, the MSD model parameters, these are the mass, damping and stiffness. The mass of the participants is measured and directly used as the mass in the MSD model. The damping is taken from a similar speed trial estimation form Leblanc et al. [12]. The stiffness is included as a state in the filter architecture and is processed as described in Section 3.4.

3.5.2 UKF parameters

There are three UKF parameters that need to be set, namely α, β and κ. The values shown in Table 1 are commonly used in the unscented kalman filter. A small α ensures tight grouping of the sigma points, $\beta = 2$ is optimal for gaussian distributions and κ is usually set to 0 [26].

3.5.3 Noise covariance matrices

Figure 2 shows that two of the required inputs of this model are the measurement noise and the unmeasured process covariances. These are implemented in the model in the form of a measurement noise covariance matrix ($\mathbf{R}$) and for each of the filters a process noise covariance matrix ($\mathbf{Q}$). Since the measurement and process noise are not known parameters in this instance they have to be determined experimentally. The values for the **Q** matrices were set manually to best model the waveform shape. The ratio between the **R** and **Q** influences how much the estimation is influenced by model and measurement. For the performance of the filter the ratio between these matrices is crucial. Because of this the **R** matrix was optimized using a Bayesian optimization scheme.

3.5.4 Initial values states and covariance

The initial values of the states are roughly estimated based on the order of the states evaluated during previous processing, because the displacement, velocity, and input force remained relatively small these were initially set at 0 to mimic a static starting position. The stiffness varies during a step cycle, however this variation is relatively small compared to its absolute value. The starting value used by Leblanc et al. [12] turned out to be appropriate for the data in this study as most stiffness values settled around this value. By choosing appropriate initial covariances the filter can move from the initial value to the filters estimates in the desired period. All initial covariance values were set manually with the focus on quick convergence of the states to the filter estimate without reaching instability.

Parameter	**Definition**	**Value**
Mass (m)	Participant body mass	Variable (per participant)
Damping (c)	Fixed damping coefficient	300 Ns/m
Alpha (α)	UKF parameter	1e-3
Beta (β)	UKF parameter	2
Kappa (κ)	UKF parameter	0
Initial state (X)	$[q,\ \dot{q},\ k,\ F]^T$	$\left[0,\ 0,\ 2 \cdot 10^4,\ 0\right]^T$
Initial covariance (P)	$\mathrm{diag}(\sigma_q^2,\ \sigma_{\dot{q}}^2,\ \sigma_k^2,\ \sigma_F^2)$	$\mathrm{diag}\left(10,\ 10,\ 1 \cdot 10^7,\ 100\right)$
Process noise (Q)	$\mathrm{diag}(\sigma_q^2,\ \sigma_{\dot{q}}^2,\ \sigma_k^2,\ \sigma_F^2)$	$\mathrm{diag}\left(1 \cdot 10^{-5},\ 1 \cdot 10^{-5},\ 1 \cdot 10^{-3},\ 207\right)$
Measurement noise (R)	GRF measurement variance	$\mathrm{diag}\,(130)$

Table 1: Values used for the model, filter parameters and matrices in the dual-Kalman filter estimation of vGRF

3.6 Reference method

For comparison a simple Newtonian method is implemented. Using the same sensor and data processing, GRF is estimated according to newtons second law:

$$F(t) = ma \tag{23}$$

The data is filtered using a 2nd order low pass Butterworth filter with a cut-off frequency of $5Hz$. This frequency is optimized in the same way as the dual-Kalman filter. After filtering the data the eGRF is determined using Equation 23. By comparing the results of the Kalman filter architecture with this method the benefits and drawbacks that come with the added complexity can be evaluated.

3.7 Performance evaluation

The main metric used to quantify the performance of the implemented method is the root mean square error (RMSE) between the eGRF and the GRF from the instrumented treadmill (mGRF). RMSE indicates the accuracy of the eGRF shape and amplitude during the whole gait phase. For the calculation of the RMSE only the stance phase is included as the flight phase GRF is assumed to be 0. To prevent the convergence of the stiffness from impacting the RMSE the estimation was rerun with the previously found stiffness values. As RMSE is the main performance metric it is used as the objective in the optimization of noise matrices as described in Section 3.5.3. For this optimization a training/test data split of 75%/25% was applied to prevent overfitting of the model.

Two other performance metrics are used to evaluate the model. Namely the mean of both the absolute and relative peak error (mean peak error) and the Pearson's correlation coefficient. The mean peak error gives a good indication of the accuracy of the peak GRF which on its own can give valuable insight to fatigue. Pearson's coefficient gives insight on the correlation between the eGRF and mGRF and thus the accuracy of the waveform shape of the eGRF while neglecting its amplitude.

4 Results

4.1 participant exclusion

One of the measurements is excluded from the results. For this participants the waveform of the measured acceleration in the sternum sensor consistently goes to $0BW$ in the middle of the step cycle following a sinusoidal shape. The measured behavior is unexplainable from a biomechanical standpoint and is not seen in any other participant. Most likely this is behavior is caused by imperfect sensor connections, as the wires connected to the legs are moving rapidly and need to be strongly secured.

4.2 Dual-Kalman filter method performance

On average the dual Kalman filter method achieved an average RMSE of $0.206BW$. Table 2 shows all performance metrics per participant.

Participant	RMSE (BW)	Absolute mean peak error (BW)	Relative mean peak error (%)	Pearson's r
1	0.206	0.1023	3.929	0.97
2	0.172	0.0477	2.156	0.97
3	0.213	0.0660	2.784	0.96
4	0.242	0.0389	1.658	0.95
5	0.277	0.0540	2.127	0.94
6	0.160	0.0628	2.788	0.98
7	0.168	0.0688	2.878	0.98
8	0.231	0.1037	4.485	0.96
9	0.248	0.4088	20.108	0.96
10	0.203	0.0363	1.755	0.96
11	0.202	0.1152	5.395	0.96
12	0.249	0.0949	3.941	0.95
Mean	0.214	0.1000	4.500	0.962

Table 2: Performance metrics per participant and their mean

In Figure 3 the eGRF is shown against mGRF for each of the contestants. Here you can see the visual difference between the estimated and measured GRF. The accuracy of the estimated GRF varies between participants. However, it can be seen all impact peaks are estimated to late and mostly underestimated in their amplitude.

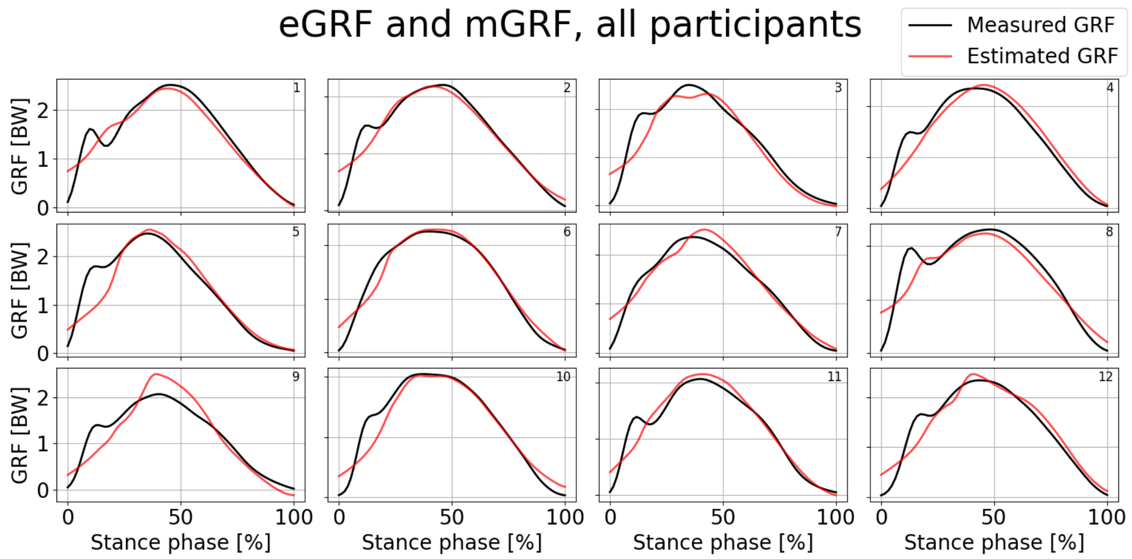

FIGURE 3: eGRF compared to mGRF for every participant

Below a typical example of the convergence of the stiffness is shown for one of the participants. For all participant the stiffness has converged after 10 seconds.

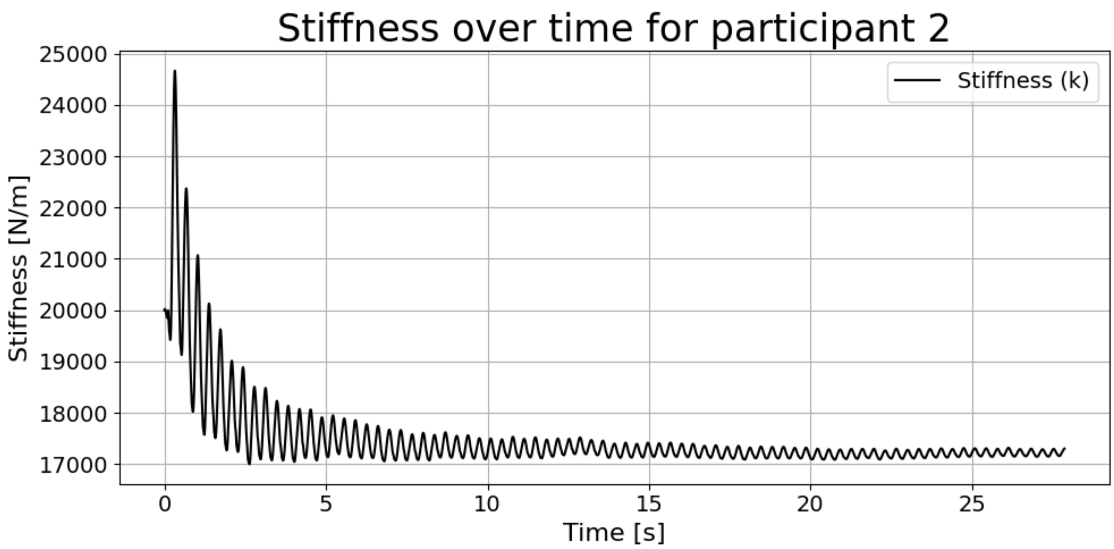

FIGURE 4: Stiffness parameter of the mass spring damper model, predicted as part of the augmented state vector in the UKF

The stiffness varies significantly per participant, an overview of all converged stiffness values is shown in Table 3. The average stiffness is $22.864kN/m$ with a standard deviation of $4.252kN/m$.

Participant	1	2	3	4	5	6	7	8	9	10	11	12
Stiffness $[kN/m]$	20.32	17.22	25.88	21.39	26.12	23.33	20.15	17.22	33.23	20.71	24.78	24.04

TABLE 3: Stiffness per participant

4.3 Newtonian method performance

For comparison the overall performance of the simple Newtonian method presented in Section 3.6 is shown in Table 4.

RMSE (BW)	**Absolute mean peak error (BW)**	**Relative mean peak error (%)**	**Pearson's r**
0.178 ± 0.044	0.1310 ± 0.0809	5.793 ± 4.081	0.978 ± 0.010

TABLE 4: Performance metrics simple Newtonian method with standard deviation

For comparison of the performance of the Newtonian method below a step cycle and its eGRF is presented below. Both a step cycle with and without a strong impact peak are shown to allow comparison of the performance of the dual-Kalman filter method for different stride patterns.

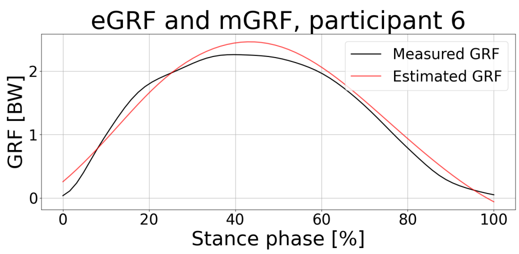

(A) eGRF compared to mGRF, participant 6

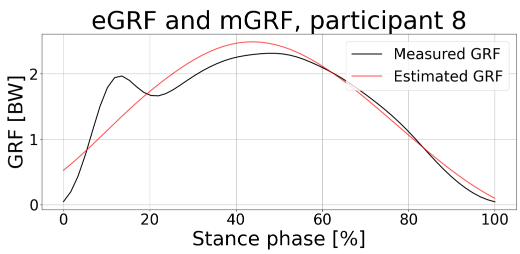

(B) eGRF compared to mGRF, participant 6

FIGURE 5: eGRF compared to mGRF using the Newtonian method. Participant 6 and 8 are presented to show the model performance for different stride patterns

5 Discussion

The goal of this study was to evaluate the application of a dual-Kalman filter as described by Leblanc et al. [12] on a single sternum placed sensor setup. With the end goal of achieving accurate vGRF estimation with limited sensor equipment, which can then be used for injury prevention.

The dual-Kalman filter method achieved an average RMSE of 0.214 ± 0.035BW, an average absolute mean peak error of 0.1000 ± 0.0965BW, a relative absolute mean peak error of 4.500 ± 4.833% and a Pearson's correlation coefficient of 0.962 ± 0.011. As can be seen in Figure 3 the filter is not able to precisely match all the characteristics of the GRF waveform. For a good part of the participants the active peak is estimated fairly accurately while the impact peak is underestimated as well as delayed for all participants. It is expected that a single IMU setup has difficulty estimating the impact peak as most of the initial impact force is absorbed in the lower body and is thus not as prominently seen in the acceleration of the upper trunk. This causes the accelerations of the lower extremities of the body to be highly correlated with the impact peak characteristics while the acceleration of the upper body has a lower correlation [14]. Furthermore, the delay between the true impact peak and its representation in the measured acceleration is explained by the time it takes for the forces to propagate through the body. While these two factors make it difficult to estimate the impact peak accurately using only a sensor on the upper trunk, the dynamic nature of the Kalman filter should allow for better filtering of the impact peak compared to a low pass filter as used in the Newtonian method. Figure 3 shows that for participants 1 and 8 a small impact peak is estimated. While this is a closer representation of the impact peak than estimated by the Newtonian method as shown in figure 5b, the inaccuracy that is still present in these two cases combined with the the impact peak missing from the other estimations shows that in its current form this method does not provide a significant benefit over the Newtonian method for estimation of the impact peak.

As for the overall performance of the filter its RMSE is higher compared to the Newtonian method (0.214 compared to 0.178). For both absolute and relative peak error the dual Kalman filter performs slightly better compared to the Newtonian method (0.1000 and 4.500 compared to 0.1310 and 5.793). Lastly, the p correlation is slightly better using the Newtonian method (0.978 for the Newtonian method and 0.962 for the dual-Kalman filter method). These metrics show that only in the estimation of the peak GRF the dual-Kalman structure is superior. While accurate estimation of the peak GRF is useful by itself, it is important to mention that both estimation methods were optimized based on RMSE and not mean peak error. Because of this it is hard to conclude which method would be more suitable for estimating peak GRF. As for the other metrics the Newtonian method while computationally more simple achieves a noticeably lower RMSE and also has a slightly higher Pearson's coefficient, thus in general outperforming the dual-Kalman filter method.

Both the dual-Kalman filter method and Newtonian method should also be compared to other literature. Firstly the performance is evaluated against a multi sensor setup. While a single sensor setup is expected to be outperformed by a multi sensor setup, this can give useful insight in to the trade off between ease of use and accuracy. Scheltinga et al. [19] achieved an average RMSE of $0.157BW$ at the same running speed. While this is significantly outperforming the dual-Kalman filter method the Newtonian method compares relatively well in this error metric, achieving a 13.4% higher RMSE . More noticeable is the performance deficit of the peak error metrics, where Scheltinga et al. [19] an absolute and relative mean peak error of $0.085BW$ and 3.68%. Here the dual-Kalman filter achieves 17.7% higher absolute mean peak error and the Newtonian method a 54.1% higher absolute mean peak error, the relative mean peak error differences are in the same order. Lastly, the p-correlation is 0.98 in the multi sensor setup.

The dual-Kalman filter is also compared to the results found by Leblanc et al. [12] using the same method. While the model was successfully validated by Leblanc, the exact performance is hard to compare due to a mismatch in error parameters since RMSE is not included in the paper from Leblanc et al. Visually comparing the step cycles and their estimation the results from Leblanc show a similar amount of imperfections in the estimation of vGRF. It is notable that most of the error in the paper by Leblanc occurs in the decay after the active peak while most of the error in the results from this study comes from the passive peak. A parameter that can be compared is the RMSE of the peak, here this study outperforms the study be Leblanc et al. (0.11 ± 0.09 compared to 0.19 ± 0.04) although the variance is higher. There are however some notable differences between the two studies. Firstly, the sensor location is different (sternum compared to sacrum). Although the torso is fairly rigid there is like some acceleration absorbed in between these points. This should allow the sacrum sensor to slightly better estimate the impact peak. Secondly, the running style of the participants varies between the studies. This study contains mostly heel-strike runners showing clear impact peaks. Where although not stated the GRF waveforms seem to indicate a more mid- or forefoot running style in the participants in the study be Leblanc et al. Since the impact peak is difficult to estimate using a single sensor setup this should allow for a higher accuracy estimating vGRF of non-heel-strike runners. Lastly, the sample frequency of the used equipment is higher in this study for both the IMU and instrumented treadmill. While a lower sample frequency of the IMU is more representative to the IMU's used in commercial equipment, a lower sampling frequency for the reference signal could miss out on some high frequency behavior.

One of the theoretical strengths of the dual-Kalman filter approach is the estimation of the stiffness parameter. This parameter is influenced by many factors such as running form, running surface and shoe type. As these factors change from person to person and might even change over different training sessions the ability of the filter to account for these changes is a valuable advantage. However, in the current implementation it also shows some disadvantages. The participants for which the stiffness converges to higher values a higher peak error is observed, most prominently visible for participant 9 which has a significantly higher estimated stiffness as well as a high peak error. Implementing a predefined stiffness (such as $20kN/m$) in a similar filter structure results in a higher peak accuracy since it consistently dampens the peak to the same degree, however it also leads to a higher RMSE. This does show that the dynamic estimation of the stiffness is beneficial for a low RMSE value compared to a similar method without dynamic stiffness.

Currently the dual-Kalman filter does have some limitations. The model includes a single mass spring damper model while the body consists of multiple moving segments with each their own mass. Since the impact peak is mainly absorbed in the lower body [19] the use of only a single mass is unable to accurately model both peaks. The impact peak is most prevalent in heel strike runners. This leads to the current model modeling mid- and forefoot-strike runners better than heel-strike runners. As most runners use a heel-strike ($75\% - 95\%$) [27] it is desirable to improve the accuracy of GRF estimation for heel-strike runners specifically. To do this a more complex model could be implemented using a similar filter structure. Here a double mass spring damper model could be used [28] to increase the ability of the model to capture the impact peak or for even higher accuracy of the runners model a higher order MSD model could be implemented as proposed by Zanetti et al. [29].

Another limitation of the current structure is that it only estimates vertical GRF, ignoring forces in the mediolateral and posterior-anterior direction. While the forces in these directions are relatively small [11] compared to the vGRF they still add to the total biomechanical load. Especially when looking at sprinting and direction changes while running these forces can add up to a significant addition in biomechanical load that is currently neglected. In future implementing a 3D GRF estimation could make the model more representative of the total biomechanical load on the body. This could also make it more suitable for use in other sports where sprinting and direction changes are more common such as football.

Future research could be done to improve the presented method. For the goal of accurately estimating the impact peak for heel-strike runners there are currently two main problems. Firstly, the inability for the model to represent both passive and active peak, which could possibly be improved by implementing a more complex model as described previously. Secondly, the underrepresentation of the passive peak in the acceleration measured on the sternum. If a single sensor setup is desired future research could be done using other sensor locations closer to or on the lower body where the passive peak is more present, otherwise a multiple sensor setup can be applied as shown by Scheltinga et al. [19]. To make the model more generally applicable more research should be done to estimate the mediolateral and posterior-anterior components of GRF. Furthermore, the method should be validated at higher running speeds since accuracy of the vGRF estimation tends to decrease as speed increases [11].

6 Conclusion

The goal of this study was to evaluate the application of a dual-Kalman filter as described by Leblanc et al. [12] on a single sternum placed sensor setup. With the end goal of achieving accurate vGRF estimation with limited sensor equipment, which can than be used for injury prevention. The GRF estimation using this setup was not as accurate compared to a more simple Newtonian method. A similar accuracy as Leblanc et al. was achieved. The application of the method in its current form does not validate its use over other single sensor estimation methods. Using a more complex model, this method could improve performance and be especially useful for the estimation of the impact peak. To verify this further research is needed. The inclusion of dynamic stiffness estimation could also be a benefit over other methods which do not allow for dynamic stiffness estimation, as stiffness varies significantly from person to person. These two factors could support further research into the dual-Kalman filter method, however in the current form of the method described in this paper the presented method does not provide a better insight than other methods such as the Newtonian method and thus does not provide an improved estimation of biomechanical load with the goal of reducing injury risk.

References

[1] Darren ER Warburton et al. "A systematic review of the evidence for Canada's Physical Activity Guidelines for Adults". In: *International Journal of Behavioral Nutrition and Physical Activity* 7.1 (2010), p. 39. ISSN: 1479-5868. DOI: 10.1186/1479-5868-7-39. URL: http://ijbnpa.biomedcentral.com/articles/10.1186/1479-5868-7-39.

[2] Jessica S. Gorzelitz. "Applied Physical Activity Epidemiology: Relationship of Physical Activity and Exercise Exposures with Health Outcomes". In: 2024, pp. 23–36. DOI: 10.1007/7854{_}2024{_}489. URL: https://link.springer.com/10.1007/7854_2024_489.

[3] Welzijn en Sport Ministerie van Volksgezondheid. "Cijfers en feiten sport en bewegen". In: (). URL: https://www.loketgezondleven.nl/gezondheidsthema/sport-en-bewegen/cijfers-en-feiten-sport-en-bewegen.

[4] Ryan M. Hulteen et al. "Global participation in sport and leisure-time physical activities: A systematic review and meta-analysis". In: *Preventive Medicine* 95 (Feb. 2017), pp. 14–25. ISSN: 00917435. DOI: 10.1016/j.ypmed.2016.11.027. URL: https://linkinghub.elsevier.com/retrieve/pii/S0091743516303838.

[5] Duck-chul Lee et al. "Leisure-Time Running Reduces All-Cause and Cardiovascular Mortality Risk". In: *Journal of the American College of Cardiology* 64.5 (Aug. 2014), pp. 472–481. ISSN: 07351097. DOI: 10.1016/j.jacc.2014.04.058. URL: https://linkinghub.elsevier.com/retrieve/pii/S0735109714027466.

[6] Freya Oswald et al. "A Scoping Review of the Relationship between Running and Mental Health". In: *International Journal of Environmental Research and Public Health* 17.21 (Nov. 2020), p. 8059. ISSN: 1660-4601. DOI: 10.3390/ijerph17218059.

[7] Bin Feng et al. "INFLUENCE OF LONG-DISTANCE RUNNING ON MENTAL HEALTH AND POSITIVE SPORTS EMOTIONS OF COLLEGE STUDENTS". In: *REVISTA ARGENTINA DE CLINICA PSICOLOGICA* (2020). ISSN: 18517951. DOI: 10.24205/03276716.2020.296. URL: https://www.revistaclinicapsicologica.com/article.php?doi=10.24205/03276716.2020.296.

[8] Daphne Menheere et al. "Runner's Perceptions of Reasons to Quit Running: Influence of Gender, Age and Running-Related Characteristics". In: *International Journal of Environmental Research and Public Health* 17.17 (Aug. 2020), p. 6046. ISSN: 1660-4601. DOI: 10.3390/ijerph17176046. URL: https://www.mdpi.com/1660-4601/17/17/6046.

[9] Alan Hreljac. "Etiology, Prevention, and Early Intervention of Overuse Injuries in Runners: a Biomechanical Perspective". In: *Physical Medicine and Rehabilitation Clinics of North America* 16.3 (Aug. 2005), pp. 651–667. ISSN: 10479651. DOI: 10.1016/j.pmr.2005.02.002. URL: https://linkinghub.elsevier.com/retrieve/pii/S1047965105000197.

[10] Christine Sapienza and Bari Hoffman. *Respiratory muscle strength training*. 2021.

[11] Bouke L. Scheltinga et al. "Estimating 3D ground reaction forces in running using three inertial measurement units". In: *Frontiers in Sports and Active Living* 5 (May 2023). ISSN: 2624-9367. DOI: 10.3389/fspor.2023.1176466. URL: https://www.frontiersin.org/articles/10.3389/fspor.2023.1176466/full.

[12] Benjamin LeBlanc et al. "Continuous estimation of ground reaction force during long distance running within a fatigue monitoring framework: A Kalman filter-based model-data fusion approach". In: *Journal of Biomechanics* 115 (Jan. 2021), p. 110130. ISSN: 00219290. DOI: 10.1016/j.jbiomech.2020.110130. URL: https://linkinghub.elsevier.com/retrieve/pii/S0021929020305546.

[13] Xianta Jiang et al. "Estimating Vertical Ground Reaction Force during Walking Using a Single Inertial Sensor". In: *Sensors* 20.15 (Aug. 2020), p. 4345. ISSN: 1424-8220. DOI: 10.3390/s20154345.

[14] Eoin W. Doyle et al. "Sensor location influences the associations between IMU and motion capture measurements of impact landing in healthy male and female runners at multiple running speeds". In: *Sports Biomechanics* (Jan. 2024), pp. 1–15. ISSN: 1476-3141. DOI: 10.1080/14763141.2023.2298954.

[15] Marek Pańtak. "Ground Reaction Forces Generated by Runners—Harmonic Analyses and Modelling". In: *Applied Sciences* 10.5 (Feb. 2020), p. 1575. ISSN: 2076-3417. DOI: 10.3390/app10051575.

[16] Brandon Oubre et al. "Estimating Ground Reaction Force and Center of Pressure Using Low-Cost Wearable Devices". In: *IEEE Transactions on Biomedical Engineering* 69.4 (Apr. 2022), pp. 1461–1468. ISSN: 0018-9294. DOI: 10.1109/TBME.2021.3120346. URL: https://ieeexplore.ieee.org/document/9573257/.

[17] Andrea Ancillao et al. "Indirect Measurement of Ground Reaction Forces and Moments by Means of Wearable Inertial Sensors: A Systematic Review". In: *Sensors* 18.8 (Aug. 2018), p. 2564. ISSN: 1424-8220. DOI: 10.3390/s18082564. URL: https://www.mdpi.com/1424-8220/18/8/2564.

[18] Marion Mundt et al. "Estimating Ground Reaction Forces from Two-Dimensional Pose Data: A Biomechanics-Based Comparison of AlphaPose, BlazePose, and OpenPose". In: *Sensors* 23.1 (Dec. 2022), p. 78. ISSN: 1424-8220. DOI: 10.3390/s23010078. URL: https://www.mdpi.com/1424-8220/23/1/78.

[19] Bouke L. Scheltinga et al. "Estimating Vertical Ground Reaction Force during Running with 3 Inertial Measurement Units". In: *Journal of Biomedical Engineering and Biosciences* (2022). ISSN: 25644998. DOI: 10.11159/jbeb.2022.006. URL: https://jbeb.avestia.com/2022/006.html.

[20] Eva Dorschky et al. "Comparing sparse inertial sensor setups for sagittal-plane walking and running reconstructions". In: *Frontiers in Bioengineering and Biotechnology* 13 (Feb. 2025). ISSN: 2296-4185. DOI: 10.3389/fbioe.2025.1507162. URL: https://www.frontiersin.org/articles/10.3389/fbioe.2025.1507162/full.

[21] B. Song et al. "Estimating Ground Reaction Forces From Inertial Sensors". In: *IEEE Transactions on Biomedical Engineering* 72.2 (Feb. 2025), pp. 595–608. ISSN: 0018-9294. DOI: 10.1109/TBME.2024.3465373. URL: https://ieeexplore.ieee.org/document/10684546/.

[22] Claudio Urrea and Rayko Agramonte. "Kalman Filter: Historical Overview and Review of Its Use in Robotics 60 Years after Its Creation". In: *Journal of Sensors* 2021.1 (Jan. 2021). ISSN: 1687-725X. DOI: 10.1155/2021/9674015.

[23] Sharon R. Bullimore and Jeremy F. Burn. "Ability of the planar spring–mass model to predict mechanical parameters in running humans". In: *Journal of Theoretical Biology* 248.4 (Oct. 2007), pp. 686–695. ISSN: 00225193. DOI: 10.1016/j.jtbi.2007.06.004. URL: https://linkinghub.elsevier.com/retrieve/pii/S0022519307002834.

[24] R. Blickhan. "The spring-mass model for running and hopping". In: *Journal of Biomechanics* 22.11-12 (Jan. 1989), pp. 1217–1227. ISSN: 00219290. DOI: 10.1016/0021-9290(89)90224-8. URL: https://linkinghub.elsevier.com/retrieve/pii/0021929089902248.

[25] V.K. Dertimanis et al. "Input-state-parameter estimation of structural systems from limited output information". In: *Mechanical Systems and Signal Processing* 126 (July 2019), pp. 711–746. ISSN: 08883270. DOI: 10.1016/j.ymssp.2019.02.040. URL: https://linkinghub.elsevier.com/retrieve/pii/S0888327019301190.

[26] E.A. Wan and R. Van Der Merwe. "The unscented Kalman filter for nonlinear estimation". In: *Proceedings of the IEEE 2000 Adaptive Systems for Signal Processing, Communications, and Control Symposium (Cat. No.00EX373)*. IEEE, pp. 153–158. ISBN: 0-7803-5800-7. DOI: 10.1109/ASSPCC.2000.882463. URL: http://ieeexplore.ieee.org/document/882463/.

[27] Joseph Hamill and Allison H. Gruber. "Is changing footstrike pattern beneficial to runners?" In: *Journal of Sport and Health Science* 6.2 (June 2017), pp. 146–153. ISSN: 20952546. DOI: 10.1016/j.jshs.2017.02.004.

[28] Jasper Verheul et al. "Biomechanical loading during running: can a two mass-spring-damper model be used to evaluate ground reaction forces for high-intensity tasks?" In: *Sports Biomechanics* 20.5 (July 2021), pp. 571–582. ISSN: 1476-3141. DOI: 10.1080/14763141.2019.1584238.

[29] L.R. Zanetti and M.J. Brennan. "A new approach to modelling the ground reaction force from a runner". In: *Journal of Biomechanics* 127 (Oct. 2021), p. 110639. ISSN: 00219290. DOI: 10.1016/j.jbiomech.2021.110639. URL: https://linkinghub.elsevier.com/retrieve/pii/S0021929021004097.